Journal Pre-proof

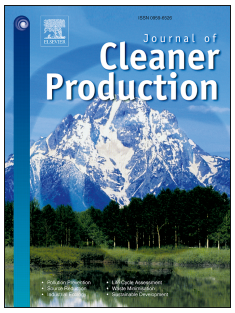

Use of Mg/Ca modified biochars to take up phosphorus from acid-extract of incinerated sewage sludge ash (ISSA) for fertilizer application

Le Fang, Jiang-shan Li, Shane Donatello, C.R. Cheeseman, Chi Sun Poon, Daniel C.W. Tsang

PII: S0959-6526(19)33723-0

DOI: https://doi.org/10.1016/j.jclepro.2019.118853

Reference: JCLP 118853

To appear in: *Journal of Cleaner Production*

Received Date: 11 December 2018

Revised Date: 24 September 2019

Accepted Date: 11 October 2019

Please cite this article as: Fang L, Li J-s, Donatello S, Cheeseman CR, Poon CS, Tsang DCW, Use of Mg/Ca modified biochars to take up phosphorus from acid-extract of incinerated sewage sludge ash (ISSA) for fertilizer application, *Journal of Cleaner Production* (2019), doi: https://doi.org/10.1016/j.jclepro.2019.118853.

Using Mg/Ca modified biochar to take up phosphorus from acid-extract of incinerated sewage sludge ash (ISSA) for fertilizer application

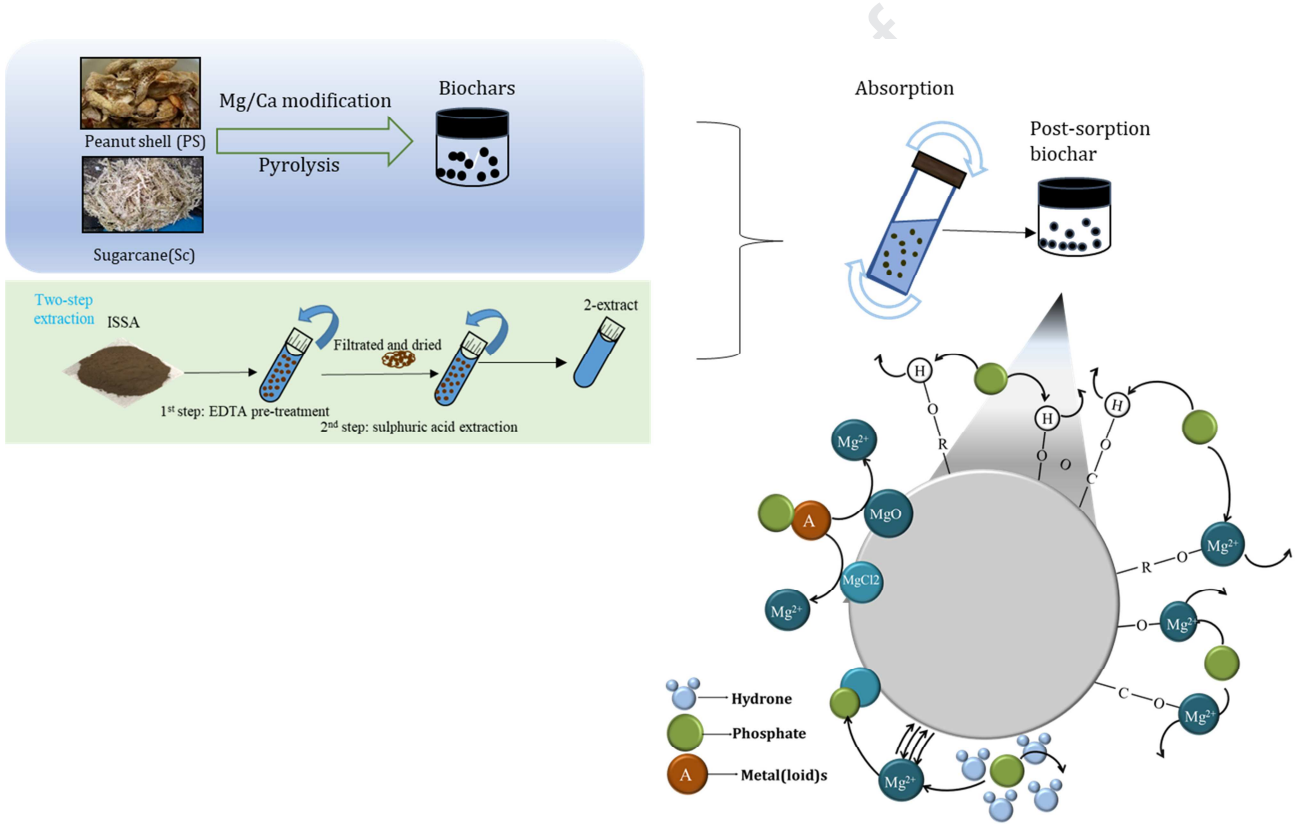

Use of Mg/Ca modified biochars to take up phosphorus from acid-extract of incinerated sewage sludge ash (ISSA) for fertilizer application

Le Fang[a,c], Jiang-shan Li[a,b,c#], Shane Donatello[e], C. R. Cheeseman[d], Chi Sun Poon[a,c*], Daniel C. W. Tsang[a]

[a] Department of Civil and Environmental Engineering, The Hong Kong Polytechnic University, Hung Hom, Kowloon, Hong Kong

[b]State Key Laboratory of Geomechanics and Geotechnical Engineering, Institute of Rock and Soil Mechanics, Chinese Academy of Sciences, Wuhan 430071, China

[c]IRSM-CAS/HK PolyU Joint Laboratory on Solid Waste Science, Hung Hom, Kowloon, Hong Kong

[d] Department of Civil and Environmental Engineering, Imperial College London, London, United Kingdom

[e] Joint Research Centre, Directorate B5 Unit. Circular Economy and Industrial Leadership, Seville, Spain

*corresponding author: cecspoon@polyu.edu.hk

[#]corresponding author: jiangshan.li@polyu.edu.hk

Abstract

Recovery of phosphorus (P) from incinerated sewage sludge ash (ISSA) by biochar is an attractive solution for mitigating the P scarcity and transferring waste to resources. This work used Mg/Ca-modified biochars to take up P from the acid-extract from ISSA at low pH (<2), which simplified the previous P recycling process. The hypothesis is to produce a P-enriched post-sorption biochar that can be directly applied as a P fertilizer. Wastes of peanut shell and sugarcane bagasse were used to synthesize Mg/Ca-modified biochars at pyrolysis temperatures of 450 ^{o}C, 700 ^{o}C and 850 ^{o}C. Preliminary results indicated Mg-modified sugarcane bagasse biochar pyrolysed at 700 ^{o}C produced optimal P-absorption. This biochar was positively charged and had a high specific surface area (1440 m^2/g), consistent with a layered porous structure. The optimal biochar showed rapid adsorption of P which could be described by the pseudo-second-order model. Successful adsorption of P from the acid-extract by the optimal biochar was mainly due to chemical precipitation and its adsorption capacity is 129.79 mg P/g biochar.

Keywords: fertilizer; phosphorus; sewage sludge ash; biochars; peanut shells

1. Introduction

Large amounts of sewage sludge are produced worldwide every year and they are dominantly agriculture applied and landfilled worldwide (Christodoulou & Stamatelatou, 2016; Lundin et al., 2004). To be specific, in China, approximately landfilled and agriculture take up 31.03% and 44.83%, respectively (Wang et al., 2006; Xu et al., 2014). However, using of the sewage sludge as fertilizers is increasingly inhibited around the world due to their potential impact to the environment. Incineration of sewage sludge is becoming more popular especially in developed cities due to its better pollution control and potentials for volume reduction, landfill capacity saving and energy recovery (Lundin et al., 2004). The Hong Kong Government has constructed a sewage sludge treatment facility (T·Park) that can incinerate maximum 2,000 tons of dewatered sludge per day. Recently, the T·Park incinerates about 1500 tons of sludge per day and generates about 150 tons of incinerated sewage sludge ash (ISSA), which is currently disposed of to landfill (T·Park, 2018). Previous studies have shown that Hong Kong ISSA contains 35 g/kg of phosphorus (P), which is one of the three main inorganic nutrients used in industrial fertilizers that are essential for plant growth (P, N and K) (Cui et al., 2016; Fang et al., 2018b). Meanwhile, P recovery from ISSA is more feasible than that from sewage sludge due to P is dominantly in the form of organic-P (Cieślik & Konieczka, 2017; Tarayre et al., 2016). It is well known that economically extractable P reserves are essentially finite because they form over geological timescales. Consequently, the recovery of P from ISSA for use in fertilizers is a central objective of this study as part of the attempt to develop a circular economy for P.

Previous studies by the authors have developed an effective extraction method to obtain a P-rich acid-extract from ISSA (Fang et al., 2018a). The acid-extract needs further treatment prior to any application as a P-fertilizer due to the low P concentration and high acidity.

Biochar is a carbonaceous adsorbent characterized by high porosity, specific surface area and certain surface functional groups (Li et al., 2019; Yang et al., 2018).

Biochar can be used as a soil conditioner to retain and progressively release nutrients, improve soil fertility, increase seed germination rates, plant growth and crop yields (Glaser et al., 2002). An additional advantage of biochars compared to inorganic fertilizers is that their non-carbonized fraction may interact with soil contaminants, thereby improving the properties of soil (Ahmad et al., 2014).

The surface of biochar is negatively charged and has a low oxyanion removal capacity (Li et al., 2018; Xu et al., 2011; Yao et al., 2011). P is usually present as an oxyanion (e.g. PO_4^{3-}, HPO_4^{2-}, $H_2PO_4^-$, depending on the pH) and the P adsorption capacity of biochar must be improved by modification with metal cations like Mg^{2+}, Ca^{2+}, Fe^{3+} or Al^{3+} (Chen et al., 2011; Fang et al., 2015; Le Leuch & Bandosz, 2007; Zhang & Gao, 2013). Oxyanion removal is governed by positively charged sites formed by protonation of metal oxides in the metal-biochar composite (Li et al., 2018). Biochars modified with Mg can induce Mg-P particles formation on the surface of the biochars (Fang et al., 2014; Li et al., 2017; Yao et al., 2013) while that with Ca forms brushite ($CaHPO_4 \cdot 2H_2O$) (Antunes et al., 2017; Marshall et al., 2017; Zhang et al., 2012). Additionally, both Mg and Ca are essential elements for plant growth (Yao et al., 2013). Therefore Ca and Mg were used in this study to enhance P adsorption on the biochars.

The pyrolysis temperature has a major influence on the porosity of the formed biochar. Numerous meso-pores (between 2~ 50 nm) are generated when the pyrolysis temperature is below 500 ^oC but these tend to collapse above 600 ^oC (Fang et al., 2014; Liu et al., 2018; Tang et al., 2013). Increasing the pyrolysis temperature changes the mesopore distribution from ordered to disordered, increasing the specific surface area and the number of organic functional groups (Fang et al., 2014). Higher pyrolysis temperatures can produce biochars with enhanced physical action and reduce the interference from coexisting ions on P adsorption (Fang et al., 2014). Pyrolysis temperature of around 700 $^{\circ}C$ was reported to form biochars with higher aromaticity and lower polarities which improved sorption (Ahmad et al., 2012; Ahmad et al., 2014; Uchimiya et al., 2010b). Based on the above, pyrolysis temperatures of 450 ^oC, 700 ^oC and 850 ^oC were used in this study to determine the

most effective biochar for P-absorption.

The acid-extracts from ISSA are usually strongly acidic (pH<2). However, information is currently lacking in P-adsorption by biochar from acidic solutions. It is necessary to investigate P absorption under such acidic conditions because P can precipitate with metal(loid)s (Al, Fe, Ca, etc.) when the solution pH > 2 (Fang et al., 2018a).

Peanut shells (Ps) and sugarcane bagasse (Sc) are produced as municipal wastes from food processing in China. Biochars based on these materials have been reported to have promising P-adsorption capabilities (Xue et al., 2012; Zhang et al., 2012).

The overall objective of this study is to investigate how P rich acid extract from ISSA can be used to produce an effective biochar-based P-fertilizer. The P-extracts from ISSA by a 2-step acid-extraction procedure was used based on our previous study (Fang et al., 2018a). Experiments were performed to determine the optimal biochar production conditions and the optimal pH for P adsorption onto the biochar. The adsorption mechanisms were investigated using adsorption kinetic and isotherm models combined with spectroscopic and microscopic analysis (X-ray diffraction (XRD), scanning electron microscopy with energy dispersive X-ray spectroscopy (SEM-EDX) and Fourier transform infrared (FTIR)).

2. Materials and Methods

2.1 Preparation of biochars

Peanut shells (Ps) and sugarcane bagasse (Sc) were obtained from a food factory in Shenzhen, China. Prior to use they were thoroughly washed in deionized (DI) water, oven-dried at 105 $^{\circ}$C overnight and milled to pass through a 2 mm sieve.

Solutions of $MgCl_2$ and $CaCl_2$ were prepared by dissolving 40 g of $MgCl_2 \cdot 6H_2O$ and 50 g of $CaCl_2 \cdot 2H_2O$ (AR Grade, Fischer Scientific) separately in 60 mL of DI water (Fang et al., 2014; Zhang et al., 2012). The biomass samples were modified by soaking them in the prepared solutions for 1 h (mass to volume ratio of 1:3). The

modified biochars were separated by using a vacuum filter with Whatman No. 42 filter papers and then oven-dried at 105 ^{o}C until achieving constant mass. The Mg/Ca modified biomass samples were then pyrolysed at 450 $^{\circ}$C, 700 $^{\circ}$C or 850 $^{\circ}$C for 1 hour in an inert N_2 atmosphere. Samples were heated to the target temperatures at a heating rate of 10 ^{o}C/min and N_2 (99.9 vol. % purity) flow rate of 11 L/min was maintained in order to remove the pyrolysis off-gasses. The biochars formed were ball milled and sealed in vacuum desiccators prior to carrying out the absorption tests.

The biochars produced were labelled based on the biomass (Ps/Sc) used, the modifying solution ($MgCl_2$/$CaCl_2$) and the pyrolysis temperature (450, 700 and 850 ^{o}C). For example, Ps modified by $CaCl_2$ at 450 ^{o}C was labelled PsC450. Sc modified by $MgCl_2$ at 700 ^{o}C was labelled ScM700.

2.2 Production of P-extract

The ISSA used in this study was collected from T·Park, Hong Kong, which has been characterized in our previous studies and shown in Table S1 (Supplementary File) (Fang et al., 2018b; Li et al., 2017). And the P-extracts used in this study was produced from a 2-step leaching method using sampled ISSA under optimized conditions, as described in detail in previous studies (Fang et al., 2018a). In short, this 2-step leaching method involved pre-treatment of ISSA with 0.02 M EDTA at a liquid to solid ratio of 20:1 for 120 min followed by extraction with 0.2 M H_2SO_4 for 120-min.

The P-extract compositions are shown in Table 1, which contains P together with metal(loid)s. This 2-step leaching method produced an extract with reduced levels of contamination compared to other methods (Fang et al., 2018a).

2.3 Characteristics of biochars

The zeta potential of the biochars was determined (Brookhaven Instruments, Holtsville, NY) (Johnson et al., 1996). The organic functional groups on the biochars surfaces before and after adsorption were determined by FTIR analysis (Nicolet Nexus 410) in the range 4000-400 cm^{-1}. The pH of the biochars was evaluated at a

mass ratio of of 1:5 (dry sample: distilled water) by a pH meter (PHS-3C, LEICI). The surface area of the biochar was measured using the Brunauer-Emmett-Teller (BET) method using N_2 adsorption over a range of relative pressures (P/P_0) from 0.06 to 0.3. The crystalline phases in the ball-milled biochars were analyzed by using XRD (10-80 °) (Rigaku Smartlab, Japan). The surface morphology and chemical compositions of the biochars before and after adsorption were examined using a Tescan-vega3 SEM-EDX.

In addition, the biochars produced by the optimal modification method were measured by an elemental analyzer (Elementar vario EL) for C, H and N. The total P and metal(loid)s concentrations of the optimal biochar before and after sorption were measured after aqua-regia digestion. The P concentrations were measured using a spectrophotometer and the metal(loid)s were measured using inductively coupled plasma optical emission spectroscopy (ICP-OES, Spectoblue FMX 36), as in previous work (Fang et al., 2018b). And the limit of detection (LOD) of concerned metal(loid)s was shown in Table S2 (Supplementary file).

2.4 Selection of the optimal adsorbent

The effect of biomass type, pretreatment method and pyrolysis temperature of biochars on P removal from the acid-extract was studied using ten different biochars (Ps700, PsM700, PsC450, PsC700, PsC850, Sc700, ScM450, ScM700, ScM850 and ScC700). Two replicates were carried out for each test and additional replicates were performed whenever the deviation was higher than 5%. To avoid the influencing effect of P-extract characteristics and increase the effect of the biochar types on P adsorption, the P-extract was diluted 4 times and adjusted to pH 2 prior to the absorption tests.

A mixture of 0.1 g of biochar and 10 mL of P-extract was continuously agitated using an end-to-end shaker at room temperature (23 ± 2 °C) for 24 h. The mixture was then centrifuged at 4000 rpm for 5 min and the supernatant was filtered through a 0.45 μm mixed cellulose ester membrane filter prior to P and metal(loid)s analysis by ICP-OES.

The removal capacity (Q_e in mg-P/g dry biochar) of P and meta(loid)s was calculated using Eq. (1):

$$Q_e = \frac{(C_0 - C_e)V}{m} \quad (1)$$

where, C_0 (mg/L) is the initial concentration of P or metal(loid)s in the P-extract before adsorption, C_e (mg/L) is the equilibrium concentration of P or metal(loid)s in the P-extract after adsorption, V (L) is the volume of P-extract and m (g) is the mass of biochar used.

2.5 Adsorption tests

(a) Effect of initial pH on P-extract

Based on the results in Table 2, biochars of PsM700 and ScM700 were selected as the optimal P adsorbents and they were used in the absorption tests carried out at room temperature. The 4 times diluted P-extracts with different pH (1, 1.3, 1.6 and 2) were used to evaluate the effect of pH on P adsorption. The pH of the extract was adjusted by adding either 1 M NaOH or HCl. Transformation between different forms of phosphate (H_3PO_4, $H_2PO_4^-$ and HPO_4^{2-}) in the pH range studied was assessed using Visual Minteq 3.1. The supernatants were collected after 24 h of absorption for P and metal(loid)s analysis.

(b) Kinetic adsorption

The P-extract was diluted 4 times and adjusted to pH 2. The absorption process was the same as in the batch sorption experiments except that the solution samples were collected after adsorption for 5, 10, 20, 40, 60, 80, 120, 240, 360, and 720 min.

Three common models were used to fit the experimental data. These were the pseudo-first-order, pseudo-second-order and intra-particle-diffusion (IPD) models (Kołodyńska et al., 2012). These are described by Eqs. (2), (3) and (4) respectively.

$$\ln(Q_e - Q_t) = \ln Q_e - K_1 t \quad (2)$$

$$\frac{t}{Q_t} = \frac{1}{K_2 Q_e^2} + \frac{t}{Q_e} \quad (3)$$

$$Q_t = K_{id} t^{0.5} + C \quad (4)$$

where, Q_e (mg/g) is the P adsorption capacity at equilibrium; Q_t (mg/g) represents the P uptake at time t; K_1 (min^{-1}), K_2 ($g \cdot mg^{-1}min^{-1}$) and K_{id} ($mg \cdot g^{-1}min^{-1/2}$) are rate constants, C is the intercept.

(c) Adsorption isotherms analysis

Adsorption isotherms were obtained using a range of different concentrations (3-5800 mg/L) of the P-extract. To obtain higher concentration of P-extract compared with the alluded P-extract, 2.5 g of ISSA was dissolved in 20 mL of acid. While a lower concentration of P-extract was produced by dilution. Supernatants were collected after 24 h of absorption.

Langmuir, Freundlich and Sips models (Eqs. (5), (6) and (7) respectively) were applied to fit the adsorption isotherm data:

$$Q_e = \frac{Q_m K_L C_e}{1 + K_L C_e} \quad (5)$$

$$Q_e = K_F C_e^{\,1/n} \quad (6)$$

$$Q_e = \frac{Q_m K_s C_e^{1/n}}{1 + K_s C_e^{1/n}} \quad (7)$$

where, Q_e (mg/g) and C_e (mg/L) are the adsorbed capacity of the biochars and the concentration of P-extracts at equilibrium, respectively; K_L (L/mg), K_F ($(L/mg)^{1/n}$) and K_s ($(L/mg)^{1/n}$) are constants in these three models and n is the heterogeneity factor.

3. Results and discussion

3.1 Biochar optimization

The characteristics of the biochar (surface metal deposit, functional group and pH) determined the adsorption capacity for anions, oxyanions or cations. The modification method and pyrolysis temperature of biochar were selected based on previous studies (Ahmad et al., 2012; Ahmad et al., 2014; Antunes et al., 2017; Fang

et al., 2014; Li et al., 2017; Marshall et al., 2017; Uchimiya et al., 2010b; Yao et al., 2013; Zhang et al., 2012). The optimal P absorption biochar was obtained by comparing biochars produced from two kinds of biomass (Sc and Ps), two kinds of modification methods ($MgCl_2$ and $CaCl_2$) and three pyrolysis temperatures (450, 700 and 850 ^oC).

3.1.1 Characteristics of produced biochars

As shown in Fig.1a and 1b, the MgO was produced in the biochars treated with $MgCl_2$ (in range of 30- 80 ^{o}), while for the biochars treated with $CaCl_2$ (in range of 10-60 ^{o}), the CaO was formed only under 850 ^oC. This is because degradation of Mg(OH)Cl occurred with further transformation into MgO in the temperature range of 450-650 ^oC (Zhang et al., 2012). However, the thermal stability of $CaCl_2$ is higher than $MgCl_2$ and the formation of CaO requires pyrolysis temperatures greater than 850 ^oC (Rathod & Banerjee, 2013; Tyagi & Buddhi, 2008). In addition, higher pyrolysis temperatures caused crystallization of the biochars.

The FTIR data (as shown in Fig. 1c) detected peaks at wavenumbers of 3400 (O-H stretching), 1613 (C=O stretching), 1373 (C=C aromatic ring modes), 1130 (C-O stretching), 1057 (aliphatic C-O-C) and 850 cm^{-1} (C-Cl bending). Both biomasses were polymer-rich materials and formed biochars had many hydroxyl and aliphatic groups (Lonappan et al., 2018). The C=C peak intensities were increased after the modification of $MgCl_2$/$CaCl_2$. Impregnation with Mg slightly increased the peaks for O-H stretching which might be attributed to the change in orientation of the O-H groups induced by Mg (Wang & Wang, 2007). Organic functional C-H groups and C-Cl groups were detected at the pyrolysis temperature of 700 ^oC and these could enhance the P adsorption (Fang et al., 2014).

Treatment with $CaCl_2$ and $MgCl_2$ significantly enhanced the porous structure and biochar surface properties which increased the pH and zeta potential as shown in Table 2 (e.g. comparing the results of Ps700 with PsM700 and PsC700). The pyrolysis caused decomposition of organics and the remaining metal oxides led to an increase in the pH (Ps700 from 9.4 to 9.9 and Sc700 from 6.5 to 10.3) (Jung et al., 2016a).

Impregnation with Mg produced positively charged surfaces on the biochar while that with Ca was still slightly negative charged (increased from strong negative charged to slightly negative charged), as shown by their zeta potential values. Both of the modifications dramatically increased the BET values and pore volumes of the produced biochars. To be specific, treatment with $MgCl_2$ resulted in even higher BET surface areas (+33% and +1340% for PsM700 and ScM700 respectively) and higher pore volumes (+19% and +877% for PsM700 and ScM700 respectively) than the equivalent $CaCl_2$ treated biochar. The superior properties of $MgCl_2$ loaded biochar are related to the activation effect of $MgCl_2$ hydrates (Zhang et al., 2012), while the favorable properties of Sc-based biochar are due to the consistent layered porous structure as shown in Fig. 2.

The BET value and pore volume of the biochars were increased from 450 to 700 ^{o}C and decreased from 700 to 850 ^{o}C. This was resulted from increasing decomposition of the biochar causing greater exposure of the underlying layers and volatilization of HCl which produced more pores as the temperature was increased from 450 to 700 ^{o}C (Jung et al., 2016a). At higher pyrolysis temperatures (>700 ^{o}C) the pore structure formed started to collapse. A pyrolysis temperature of 700 ^{o}C was therefore considered to be optimal.

In summary, the amendment by $MgCl_2$ and pyrolysis at 700 ^{o}C resulted in the optimization of the biochar's physicochemical properties for P adsorption. Consequently, subsequent experiments for P adsorption used biochars ScM700 and PsM700 as the adsorbents.

3.1.2 P adsorption efficiency of biochars

The adsorption of P from the P-extract by the biochars is shown in Fig. 3. As could be expected from the results reported in section 3.1.1, amendment with $MgCl_2$ significantly enhanced the P absorption capacity of the biochars, with the highest removal associated with those had the highest BET surface areas and pore volumes. Absorption efficiency of P to these biochars were high (>80%) in acidic solutions (pH<2) and comparable to those in weak acidic solutions (Cui et al., 2016). With the

299 presence of SO_4^{2-} and other anions, the biochar modified with $MgCl_2$ showed high
300 selectivity to P. Because phosphate absorption is through the formation of inner sphere
301 complexes with oxides and hydroxides, while the absorption of SO_4^{2-} and other
302 cations is through outer-sphere complexes which could not interfere with P absorption
303 (Cui et al., 2016; Loganathan et al., 2014; Sarkar et al., 2011; Yang et al., 2018).

304 Meanwhile, the co-adsorption of metal(loid)s is shown in Fig. 3b. The biochars
305 impregnated with Mg absorbed a number of metal(loid)s from the P-extract
306 synergistically with their P adsorption. Massive dissolution of Mg/Ca from the Mg/Ca
307 modified biochars occurred, thus their concentrations are not shown. This implied the
308 significant effect of ion-exchange occurred in the adsorption process. For comparison,
309 it is worth noting that, through the same amendment method, biochars produced from
310 the biomass of Sc can adsorb more divalent metal ions while those from the biomass
311 of Ps adsorb more of trivalent metal ions. This can be related to their different
312 compositions, as shown in the total digestion results in Table 5, which compared
313 biochars of ScM700 and PsM700 before and after adsorption. As shown, except for
314 the massive presence of Mg and K, Fe was dominant in ScM700 while Ca was
315 dominant in PsM700 before absorption. This also explained why no absorption of Fe
316 was found by the Sc-based biochar. Thus, the occurrence of metal(loid)s or ligand
317 exchange was inferred during absorption, which agreed with previous findings that
318 metal(loid)s or ligands exchange played an important role in metal(loid)s absorption
319 (Cui et al., 2016; Uchimiya et al., 2010a). Because many undesirable metal(loid)s are
320 present in the divalent form, especially Zn and Cu, the difference in adsorption
321 behavior favors ScM700 over PsM700 in P absorption from the complex acid-extracts
322 (Donatello, 2009).

323

324 3.2 Effect of initial pH of P-extract on P removal

325 The pH value of the acid-extract controls P adsorption onto the biochar by
326 altering the surface charge of the biochar and P-speciation in the extract (Yao et al.,
327 2013). The co-precipitation of P with metal(loid)s (e.g. Al, Fe, Ca, etc.) occurs when
328 adjusting the pH of the P-extract to greater than 2. Only at a pH less than 2 is P freely

available to interact with the biochar surface, which is supported by the P extraction results from ISSA (Donatello, 2009; Fang et al., 2018a). Consequently, P absorption on the biochars from the extracts in the pH range of 1 - 2 was studied. In this pH range, H^+ was ionized from H_3PO_4 and induced the formation of $H_2PO_4^-$ as confirmed in the simulated data from Minteq (in Supplementary Information, Fig. S1).

As shown in Fig. 4, as the extract pH values increased from pH 1 to 1.6, P adsorption by the biochar also increased. At pH 1, phosphate mainly existed as H_3PO_4 in the P-extract. For phosphate to interact with the charged (positive zeta potential) biochar surfaces, it is necessary for them to have a partial negative charge. As the acidic extract interacted with the alkaline biochar, the aqueous environment would become less acidic (final equilibrium pH of around 6 – 7 was observed). As a result, the increasing in P adsorption was related to the increased ionization of $H_2PO_4^-$ as the pH increased. In comparison, the P absorption efficiency of ScM700 was higher than PsM700 under the same conditions.

The metal(loid)s removal ratio by the biochars in the pH range studies is shown in Fig. 4. The higher the pH of the P-extract was, the more metal(loid)s were adsorbed by the two kinds of absorption system (Kołodyńska et al., 2012). Therefore, this can be explained by the greater competition between the generally cationic metalloid ions and H^+ ions in solution. The absorption ratio of these two biochars was at the lowest at pH 1, and slowly increased till pH 1.6 and reached the highest at pH 2. Therefore, the P-extract with a lower pH produced biochars with reduced metal(loid)s. In comparison, biochar ScM700 had the advantage of absorbing P-extract at a low pH (1-1.6). This can be explained by the chelating of metal(loid)s with EDTA that might be easier to be captured by the porous media like ScM700.

To obtain high P recovery and relatively less metal(loid)s on ScM700 for using as a P-fertilizer, the P-extract with an initial pH of 1.6 is recommended as the optimum balance between the increased P adsorption and the limited metal(loid)s adsorption.

3.3 Adsorption kinetics

As shown in Fig. 5a, the adsorption kinetics of the two kinds of biochars from the P-extract were a two-stage absorption process, which consisted of a rapid initial adsorption phase of a very short duration (around 34mg/g within a few minutes), and a slow/steady adsorption phase (around 35 mg/g during the first 100 minutes). While both biochars achieved the similar total P adsorption, and the absorption of the ScM700 material was even more rapid during the initial phase than the PsM700 material that had a lower BET surface area. In the second stage, intra-particle diffusion might impede further P absorption. Because the reduction of P content in solution and the exhaustion of adsorption sites on the biochar, the absorption arrived at an equilibrium (Jung et al., 2015; Karaca et al., 2004).

Both of the absorption processes were further studied by fitting with three kinetic models separately. The pseudo-first-order model could not fit these absorption process (coefficient of determination-R^2 was lower than 0.5), thus was not shown. However, the absorption of P from the P-extract could be well fitted by the pseudo-second-order model (Table 3). And the fitted adsorption rate for ScM700 was higher than that for PsM700. Thus, P absorption was majorly controlled by chemical reaction/chemisorption, which was consistent with other previous findings (Liu, 2008; Smith et al., 2016).

3.4 Adsorption isotherms

The results of P adsorption isotherms are shown in Fig. 5b and c. When C_e is lower than 85 mg/L, there is a large capacity of biochar available for P absorption. As the C_e approaches around 260mg/L, the available P adsorption capacity begins to become saturated and reaches a steady state.

The absorption by both biochars closely fitted the Sips model but did not fit so well with the Langmuir model and showed even poorer agreement with the predictions according to the Freundlich model (Table 4). The best fitting by the Sips model suggested that the P absorption process was a multiple process, which was similar to the findings of previous research (Jung et al., 2015; Jung et al., 2016b; Xu et al., 2018). The limited fit with the Langmuir equation suggests that one of these

processes is a monolayer adsorption (Dai et al., 2014). According to the prediction of Sips model, the Q_m of ScM700 was 129.79 mg P/g biochar while the PsM700 was 111.80 mg P/g biochar. This further identified the higher adsorption capacity of ScM700 compared with PsM700.

3.5 Characteristics of the P-laden biochars and adsorption mechanism

As aforementioned, ScM700 was deemed as the optimal P adsorption biochar, thus its elemental composition and characteristics were analyzed by XRD, FTIR, SEM/EDX both before and after P adsorption.

As shown in Fig. 6, the XRD results verified the co-precipitation of P with Mg, Ca, Fe and Al on ScM700, which were consistent with the EDX analysis in Fig. 7, and also agreed with the previously implied chemisorption of P adsorption. The FTIR detected an obvious newly formed peak at 1100 cm^{-1}, which was attributed to hydro-phosphate (-HPO_4). In addition, the –OH at 3400 cm^{-1} was significantly decreased mostly due to the deprotonation during the adsorption of ions from the P-extract. As seen from the images in Fig. 7, the consistent thin flaked structure of ScM700 before adsorption (Fig. 2) was laden with small globular-like precipitates on the surface which were mainly consisted of Ca, Mg, Al, P and K. The EDX analysis indicated that the molar ratio of P/Mg was about 3, which was much higher than that of $Mg_3(PO_4)_2 \cdot 8H_2O$ (0.67), implying the P was co-precipitated with other elements apart from Mg and/or adsorbed to the charge surface sites.

The elemental composition of the post-sorption biochars was assessed by ICP analysis and the results are shown in Table 5. The acceptance criterion for P-fertilizers in China only limits the contents of As, Cd, Pb, Cr and Hg, which were not detected in the post-sorption biochars. For Cu and Zn, their concentrations in the post-sorption biochar were far lower than the fertilizer limits reported in Germany (Herzel et al., 2016) and Switzerland (Franz, 2008). As such, the P-rich ScM700 could be considered as an efficient and environmentally friendly P-fertilizer.

4. Conclusions

The results showed that the Sc-based biochar modified by $MgCl_2$ and pyrolysis at 700 ^{o}C had the optimal effect for P adsorption, due to its positive charged surface, relatively higher surface area (1440 m^2/g) and pore volume (1.6 cm^3/g). The Sips model could best fit the adsorption isotherm data and the estimated adsorption capacity of ScM700 to P in the acid-extract of ISSA was 130 mg/g biochar. Adsorption kinetics generally followed a pseudo-second-order model, which suggested that the P adsorption was dominantly controlled by chemical reaction (precipitation). To obtain a post-sorption biochar of high P purity, the initial pH of the acid-extract should be fixed at around 1.6. The adsorption of P from the acid-extract by the Mg-modified biochar was mainly attributed to the chemical precipitation of P-Mg, P-Ca, P-Al and P-Fe. The P-enriched biochar produced has potential to be a highly effective P-fertilizer because it contained abundant plant nutrients and little metal(loid)s. However, a complete agronomic evaluation of the P fertilizer produced under different soil and climatic conditions on various crops still needs to be assessed in further work.

Acknowledgements

The authors would like to thank the financial support of the Hong Kong Research Grants Council GRF (PolyU 152132/14E).

References

Ahmad, M., Lee, S.S., Dou, X., Mohan, D., Sung, J.-K., Yang, J.E., Ok, Y.S. 2012. Effects of pyrolysis temperature on soybean stover-and peanut shell-derived biochar properties and TCE adsorption in water. *Bioresour. Technol.*, 118, 536-544.

Ahmad, M., Rajapaksha, A.U., Lim, J.E., Zhang, M., Bolan, N., Mohan, D., Vithanage, M., Lee, S.S., Ok, Y.S. 2014. Biochar as a sorbent for contaminant management in soil and water: a review. *Chemosphere*, 99, 19-33.

Antunes, E., Jacob, M.V., Brodie, G., Schneider, P.A. 2017. Isotherms, kinetics and mechanism analysis of phosphorus recovery from aqueous solution by calcium-rich biochar produced from

biosolids via microwave pyrolysis. *J. Environ. Chem. Eng.*, 6(1), 395-403.

Chen, B., Chen, Z., Lv, S. 2011. A novel magnetic biochar efficiently sorbs organic pollutants and phosphate. *Bioresour. Technol.*, 102(2), 716-723.

Christodoulou, A., Stamatelatou, K. 2016. Overview of legislation on sewage sludge management in developed countries worldwide. *Water Sci. Technol.*, 73(3), 453-462.

Cieślik, B., Konieczka, P. 2017. A review of phosphorus recovery methods at various steps of wastewater treatment and sewage sludge management. The concept of "no solid waste generation" and analytical methods. *J. Clean. Prod.*, 142, 1728-1740.

Cui, X., Dai, X., Khan, K.Y., Li, T., Yang, X., He, Z. 2016. Removal of phosphate from aqueous solution using magnesium-alginate/chitosan modified biochar microspheres derived from Thalia dealbata. *Bioresour. Technol.*, 218, 1123-1132.

Dai, L., Wu, B., Tan, F., He, M., Wang, W., Qin, H., Tang, X., Zhu, Q., Pan, K., Hu, Q. 2014. Engineered hydrochar composites for phosphorus removal/recovery: Lanthanum doped hydrochar prepared by hydrothermal carbonization of lanthanum pretreated rice straw. *Bioresour. Technol.*, 161, 327-332.

Donatello, S. 2009. Characteristics of incinerated sewage sludge ashes: potential for phosphate extraction and re-use as a pozzolanic material in construction products,. in: *Department of Civil and Environmental Engineering*, Imperial College London.

Fang, C., Zhang, T., Li, P., Jiang, R.-f., Wang, Y.-c. 2014. Application of Magnesium Modified Corn Biochar for Phosphorus Removal and Recovery from Swine Wastewater. *Int. J. Env. Res. Pub. He.*, 11(9), 9217.

Fang, C., Zhang, T., Li, P., Jiang, R., Wu, S., Nie, H., Wang, Y. 2015. Phosphorus recovery from biogas fermentation liquid by Ca–Mg loaded biochar. *J. Environ. Sci-China*, 29, 106-114.

Fang, L., Li, J.-s., Donatello, S., Cheeseman, C., Wang, Q., Poon, C.S., Tsang, D.C. 2018a. Recovery of phosphorus from incinerated sewage sludge ash by combined two-step extraction and selective precipitation. *Chem. Eng. J.*, 348, 74-83.

Fang, L., Li, J.-s., Guo, M.Z., Cheeseman, C., Tsang, D.C., Donatello, S., Poon, C.S. 2018b. Phosphorus recovery and leaching of trace elements from incinerated sewage sludge ash (ISSA). *Chemosphere*, 193, 278-287.

Franz, M. 2008. Phosphate fertilizer from sewage sludge ash (SSA). *Waste Manage.*, 28(10), 1809-1818.

Glaser, B., Lehmann, J., Zech, W. 2002. Ameliorating physical and chemical properties of highly weathered soils in the tropics with charcoal-a review. *Biol. Fert. Soils*, 35(4), 219-230.

Herzel, H., Krüger, O., Hermann, L., Adam, C. 2016. Sewage sludge ash — A promising secondary phosphorus source for fertilizer production. *Sci. Total Environ.*, 542, 1136-1143.

Johnson, P.R., Sun, N., Elimelech, M. 1996. Colloid transport in geochemically heterogeneous porous media: Modeling and measurements. *Environ. Sci. Technol.*, 30(11), 3284-3293.

Jung, K.-W., Jeong, T.-U., Hwang, M.-J., Kim, K., Ahn, K.-H. 2015. Phosphate adsorption ability of biochar/Mg–Al assembled nanocomposites prepared by aluminum-electrode based electro-assisted modification method with MgCl2 as electrolyte. *Bioresour. Technol.*, 198, 603-610.

Jung, K.-W., Jeong, T.-U., Kang, H.-J., Ahn, K.-H. 2016a. Characteristics of biochar derived from marine macroalgae and fabrication of granular biochar by entrapment in calcium-alginate beads for phosphate removal from aqueous solution. *Bioresour. Technol.*, 211, 108-116.

Jung, K.W., Jeong, T.U., Kang, H.J., Chang, J.S., Ahn, K.H. 2016b. Preparation of modified-biochar from Laminaria japonica: Simultaneous optimization of aluminum electrode-based electro-modification and pyrolysis processes and its application for phosphate removal. *Bioresour. Technol.*, 214, 548-557.

Karaca, S., Gürses, A., Ejder, M., Açıkyıldız, M. 2004. Kinetic modeling of liquid-phase adsorption of phosphate on dolomite. *J. Colloid Interf. Sci.*, 277(2), 257-263.

Kołodyńska, D., Wnętrzak, R., Leahy, J.J., Hayes, M.H.B., Kwapiński, W., Hubicki, Z. 2012. Kinetic and adsorptive characterization of biochar in metal ions removal. *Chem. Eng. J.*, 197, 295-305.

Le Leuch, L., Bandosz, T. 2007. The role of water and surface acidity on the reactive adsorption of ammonia on modified activated carbons. *Carbon*, 45(3), 568-578.

Li, J.S., Xue, Q., Fang, L., Chi, S.P. 2017. Characteristics and metal leachability of incinerated sewage sludge ash and air pollution control residues from Hong Kong evaluated by different methods. *Waste Manage.*, 64, 161.

Li, L., Zou, D., Xiao, Z., Zeng, X., Zhang, L., Jiang, L., Wang, A., Ge, D., Zhang, G., Liu, F. 2019. Biochar as a sorbent for emerging contaminants enables improvements in waste management and sustainable resource use. *J. Clean. Prod.*, 210, 1324-1342.

Li, R., Wang, J.J., Zhou, B., Zhang, Z., Liu, S., Lei, S., Xiao, R. 2017. Simultaneous capture removal of phosphate, ammonium and organic substances by MgO impregnated biochar and its potential use in swine wastewater treatment. *J. Clean. Prod.*, 147, 96-107.

Li, R., Wang, J.J., Gaston, L.A., Zhou, B., Li, M., Xiao, R., Wang, Q., Zhang, Z., Huang, H., Liang, W. 2018. An overview of carbothermal synthesis of metal–biochar composites for the removal of oxyanion contaminants from aqueous solution. *Carbon*, 129, 674-687.

Liu, G., Zheng, H., Zhai, X., Wang, Z. 2018. Characteristics and mechanisms of microcystin-LR adsorption by giant reed-derived biochars: Role of minerals, pores, and functional groups. *J. Clean. Prod.*, 176, 463-473.

Liu, Y. 2008. New insights into pseudo-second-order kinetic equation for adsorption. *Colloid. Surface. A*, 320(1), 275-278.

Loganathan, P., Vigneswaran, S., Kandasamy, J., Bolan, N.S. 2014. Removal and Recovery of Phosphate From Water Using Sorption. *Crit. Rev. Env. Sci. Tec.*, 44(8), 847-907.

Lonappan, L., Rouissi, T., Brar, S.K., Verma, M., Surampalli, R.Y. 2018. An insight into the adsorption of diclofenac on different biochars: Mechanisms, surface chemistry, and thermodynamics. *Bioresour. Technol.*, 249, 386-394.

Lundin, M., Olofsson, M., Pettersson, G.J., Zetterlund, H. 2004. Environmental and economic assessment of sewage sludge handling options. *Resour. Conserv. Recy.*, 41(4), 255-278.

Marshall, J.A., Morton, B.J., Muhlack, R., Chittleborough, D., Kwong, C.W. 2017. Recovery of phosphate from calcium-containing aqueous solution resulting from biochar-induced calcium phosphate precipitation. *J. Clean. Prod.*, 165, 27-35.

Rathod, M.K., Banerjee, J. 2013. Thermal stability of phase change materials used in latent heat energy storage systems: A review. *Renew. Sust. Energ. Rev.*, 18, 246-258.

Sarkar, S., Chatterjee, P.K., Cumbal, L.H., SenGupta, A.K. 2011. Hybrid ion exchanger supported nanocomposites: Sorption and sensing for environmental applications. *Chem. Eng. J.*, 166(3), 923-931.

Smith, Y.R., Bhattacharyya, D., Willhard, T., Misra, M. 2016. Adsorption of aqueous rare earth

elements using carbon black derived from recycled tires. *Chem. Eng. J.*, 296, 102-111.

T·Park. 2018. <https://www.tpark.hk/tc/> (accessed 2018. 09.17).

Tang, J., Zhu, W., Kookana, R., Katayama, A. 2013. Characteristics of biochar and its application in remediation of contaminated soil. *J. Biosci. Bioeng.*, 116(6), 653-659.

Tarayre, C., De Clercq, L., Charlier, R., Michels, E., Meers, E., Camargo-Valero, M., Delvigne, F. 2016. New perspectives for the design of sustainable bioprocesses for phosphorus recovery from waste. *Bioresour. Technol.*, 206, 264-274.

Tyagi, V.V., Buddhi, D. 2008. Thermal cycle testing of calcium chloride hexahydrate as a possible PCM for latent heat storage. *Sol. Energ. Mat. Sol. C.*, 92(8), 891-899.

Uchimiya, M., Lima, I.M., Thomas Klasson, K., Chang, S., Wartelle, L.H., Rodgers, J.E. 2010a. Immobilization of Heavy Metal Ions (CuII, CdII, NiII, and PbII) by Broiler Litter-Derived Biochars in Water and Soil. *J. Agr. Food Chem.*, 58(9), 5538-5544.

Uchimiya, M., Wartelle, L.H., Lima, I.M., Klasson, K.T. 2010b. Sorption of deisopropylatrazine on broiler litter biochars. *J. Agr. Food Chem.*, 58(23), 12350-12356.

Wang, J., Lu, Z., Tian, S., Tao, J., 2006. Existing state and development of sludgy researches in domestic and foreign. *Mun. Eng. Technol. 24*, 140-143 (in Chinese).

Wang, S.-L., Wang, P.-C. 2007. In situ XRD and ATR-FTIR study on the molecular orientation of interlayer nitrate in Mg/Al-layered double hydroxides in water. *Colloid. Surface.*, 292(2), 131-138.

Xu, C., Chen, W., Hong, J. 2014. Life-cycle environmental and economic assessment of sewage sludge treatment in China. *J. Clean. Prod.*, 67, 79-87.

Xu, K., Lin, F., Dou, X., Zheng, M., Tan, W., Wang, C. 2018. Recovery of ammonium and phosphate from urine as value-added fertilizer using wood waste biochar loaded with magnesium oxides. *J. Clean. Prod.*, 187, 205-214

Xu, R.-k., Xiao, S.-c., Yuan, J.-h., Zhao, A.-z. 2011. Adsorption of methyl violet from aqueous solutions by the biochars derived from crop residues. *Bioresour. Technol.*, 102(22), 10293-10298.

Xue, Y., Gao, B., Yao, Y., Inyang, M., Zhang, M., Zimmerman, A.R., Ro, K.S. 2012. Hydrogen peroxide modification enhances the ability of biochar (hydrochar) produced from hydrothermal carbonization of peanut hull to remove aqueous heavy metals: Batch and column tests. *Chem. Eng. J.*, 200-202, 673-680.

Yang, Q., Wang, X., Luo, W., Sun, J., Xu, Q., Chen, F., Zhao, J., Wang, S., Yao, F., Wang, D., Li, X., Zeng, G. 2018. Effectiveness and mechanisms of phosphate adsorption on iron-modified biochars derived from waste activated sludge. *Bioresour. Technol.*, 247, 537-544.

Yao, Y., Gao, B., Chen, J., Zhang, M., Inyang, M., Li, Y., Alva, A., Yang, L. 2013. Engineered carbon (biochar) prepared by direct pyrolysis of Mg-accumulated tomato tissues: characterization and phosphate removal potential. *Bioresour. Technol.*, 138, 8-13.

Yao, Y., Gao, B., Inyang, M., Zimmerman, A.R., Cao, X., Pullammanappallil, P., Yang, L. 2011. Biochar derived from anaerobically digested sugar beet tailings: characterization and phosphate removal potential. *Bioresour. Technol.*, 102(10), 6273-6278.

Zhang, M., Gao, B. 2013. Removal of arsenic, methylene blue, and phosphate by biochar/AlOOH nanocomposite. *Chem. Eng. J.*, 226, 286-292.

Zhang, M., Gao, B., Yao, Y., Xue, Y., Inyang, M. 2012. Synthesis of porous MgO-biochar nanocomposites for removal of phosphate and nitrate from aqueous solutions. *Chem. Eng. J.*,

581 210, 26-32.
582

Using Mg/Ca modified biochar to take up phosphorus from acid-extract of incinerated sewage sludge ash (ISSA) for fertilizer application

Table 1. Characteristics of the P-extract

	pH	Concentration of major metal(loid)s (mg/L)	Concentration of minor metal(loid)s (μg/L)	Zeta potential
P-extract	1.1	Ca (2658.02), P (1282.14), Al (819.07), Mg (3.23), Fe (3.61), Zn (0.32), Cu (0.14), Mn (0.09)	As (10.61), Ni (10.83), Pb (10.22), Cr (1.31)	-1.29

Table 2. Characteristics of ten kinds of biochars

Sample	Zeta potential (mV)	pH	BET (m^2/g)	Pore volume (cm^3/g)	Sample	Zeta potential (mV)	pH	BET (m^2/g)	Pore volume (cm^3/g)
Ps700	-22.73	9.4	7.9	0.009	Sc700	-4.78	6.5	9.1	0.008
PsM700	5.76	9.9	120.6	0.109	ScC700	-0.45	10.3	100.2	0.161
PsC450	-2.97	10.0	6.1	0.030	ScM450	15.55	9.5	40.6	0.031
PsC700	-1.70	10.1	90.2	0.091	ScM700	26.25	9.6	1440.4	1.574
PsC850	-0.52	10.5	74.3	0.072	ScM850	2.85	9.8	228.74	0.243

Table 3 Adsorption kinetic parameters of P

	Pseudo-second-order			Intra-particle-diffusion		
	K_2 (g/(mg·min)	Q_e (mg/g)	R^2	K_{id} ($mg \cdot g^{-1}min^{-1/2}$)	C (mg/g)	R^2
SCM700	0.140	30.57	0.894	0.039	29.87	0.375
PSM700	0.049	30.41	0.962	0.106	28.50	0.455

Table 4 Adsorption isotherm parameters of P

Biochar	Freundlich			Langmuir			Sips			
	K_F (L/g)	1/n	R^2	K_L*10^{-2} $(L/g)^{1/n}$	Q_m (mg/g)	R^2	K_s $(L/g)^{1/n}$	1/n	Q_m (mg/g)	R^2
ScM700	12.205	0.295	0.867	0.850	133.89	0.982	0.003	1.233	129.79	0.982
PsM700	10.432	0.296	0.824	0.710	118.42	0.941	0.004	1.142	111.80	0.945

Table 5 Total concentration of elements in post-sorption biochars（mg/g）

`	K	N	P	C	H	Al	Ca	Cu	Fe	Mg	Mn	Sr	Zn	Se	Na	Sn
ScM700-bef	53.62	3.70	-	390.13	25.77	1.92	4.19	-	53.62	602.03	-	-	-	-	1.29	-
PsM700-bef	31.01	8.45	-	450.14	21.50	19.05	21.54	-	4.96	551.12	-	-	-	-	1.29	-
ScM700-aft	3.58	-	34.92	-	-	17.82	16.49	0.12	0.58	47.42	0.15	0.13	0.31	0.06	9.72	0.23
PsM700-aft	4.01	-	31.40	-	-	27.54	3.08	0.09	6.46	32.85	0.11	0.07	0.21	0.07	5.83	0.06
Fertilizer limitation																
German		-	-	-	-	-	-	5.00	-	-	-	-	1.50	-	-	-
Swiss		-	-	-	-	-	-	0.40	-	-	-	-	1.30	-	-	-

Ps: ‘bef’ represents before absorption; ‘aft’ represents after absorption.

Using Mg/Ca modified biochar to take up phosphorus from acid-extract of incinerated sewage sludge ash (ISSA) for fertilizer application

Fig. 1. XRD and FTIR spectra of biochars (a: XRD of biochars modified by $MgCl_2$; b: XRD of biochars modified by $CaCl_2$; c: FTIR of biochars)

Fig. 2. SEM-EDX analysis of biochars modified by $MgCl_2$ (a: PsM700; b: ScM700)

Fig. 3. Absorption results of various biochars (a: P; b: metal(loid)s)

Fig. 4. Effect of initial pH of the P-extract on adsorption by ScM700 and PsM700 (a and b: P and metal(loid)s adsorption by ScM700 and PsM700, respectively)

Fig. 5. Kinetic adsorption and adsorption isotherm analysis of P removal from the P-extract (a: Kinetic adsorption; b and c: adsorption isotherm analysis of ScM700 and PsM700, respectively)

Fig. 6. XRD and FTIR spectra of ScM700 before and after absorption (a: XRD; b: FTIR)

Fig. 7. SEM-EDX analysis of ScM700 after sorption (a: SEM-EDX; b: elements mapping of carbon, oxygen, magnesium, and phosphorus using EDX on SEM).

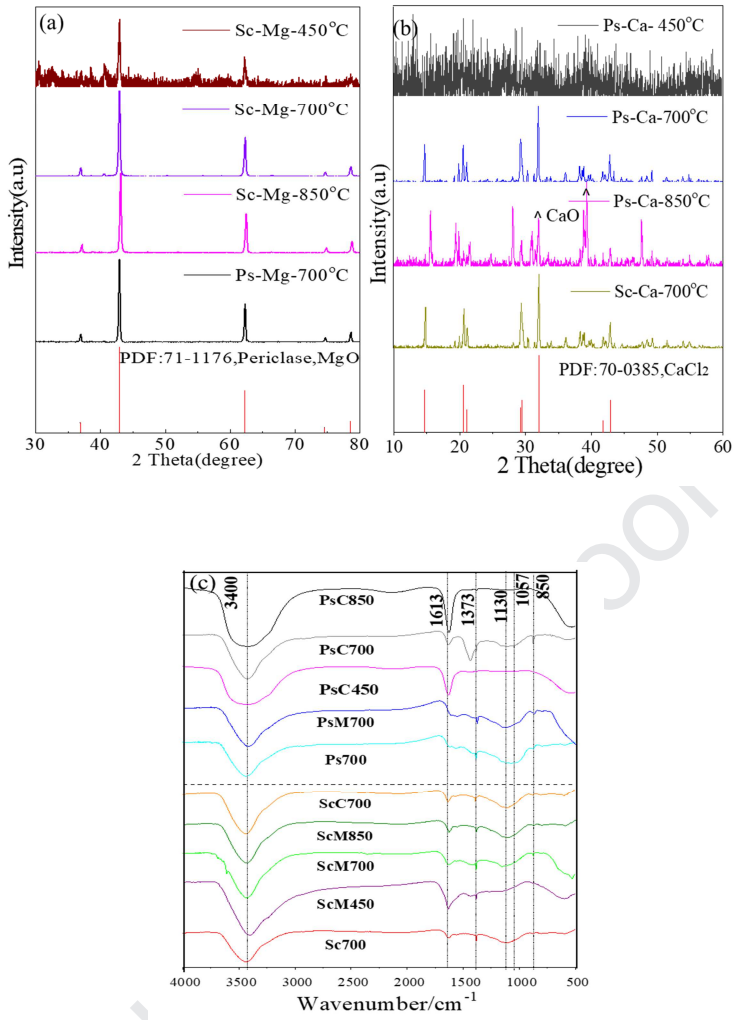

Fig. 1. XRD and FTIR spectra of biochars (a: XRD of biochars modified by $MgCl_2$; b: XRD of biochars modified by $CaCl_2$; c: FTIR of biochars)

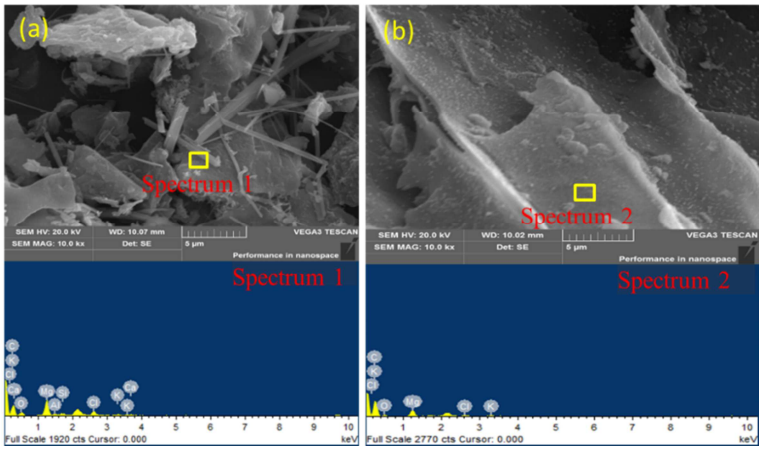

Fig. 2. SEM-EDX analysis of biochars modified by $MgCl_2$ (a, PsM700; b, ScM700)

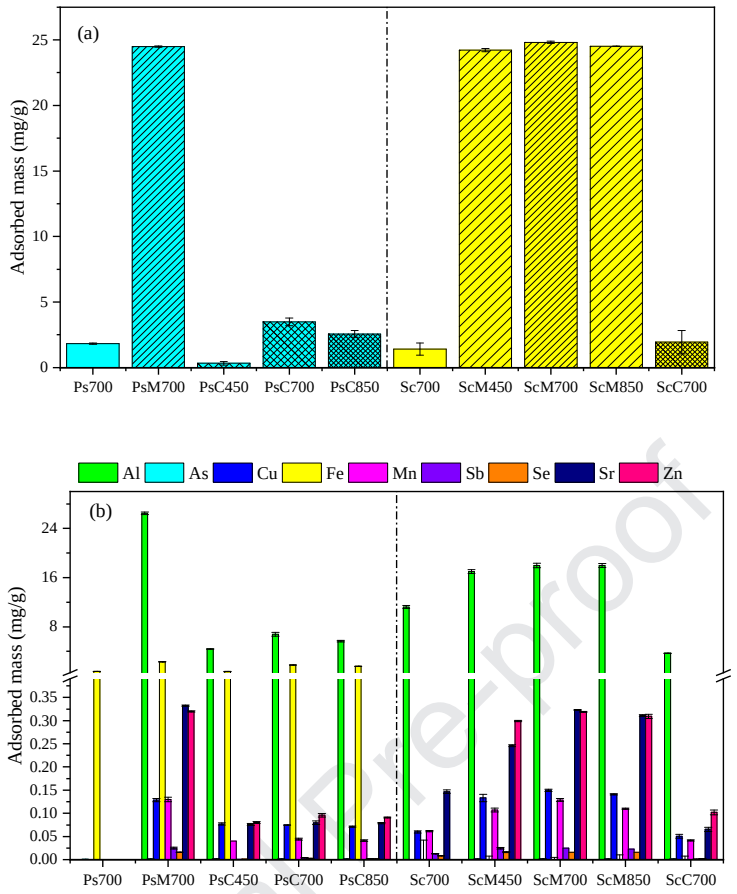

Fig. 3. Absorption results of various biochars (a: P; b: metal(loid)s)

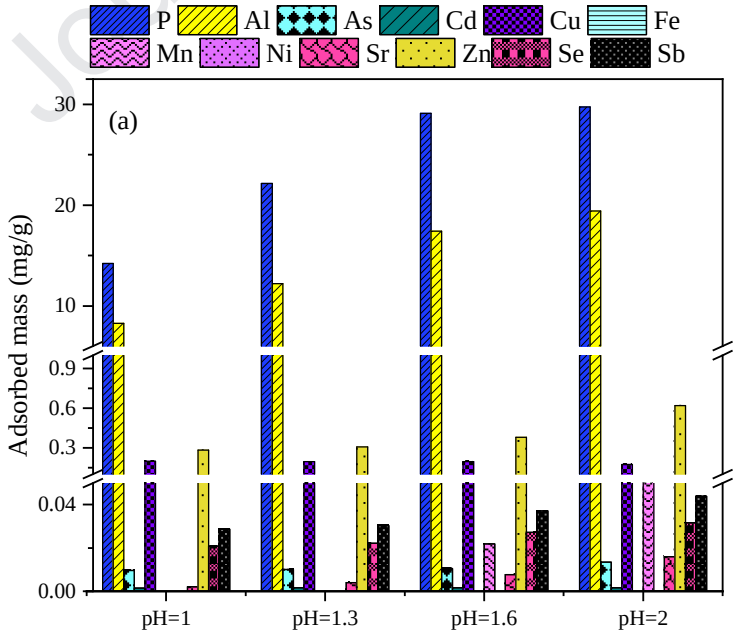

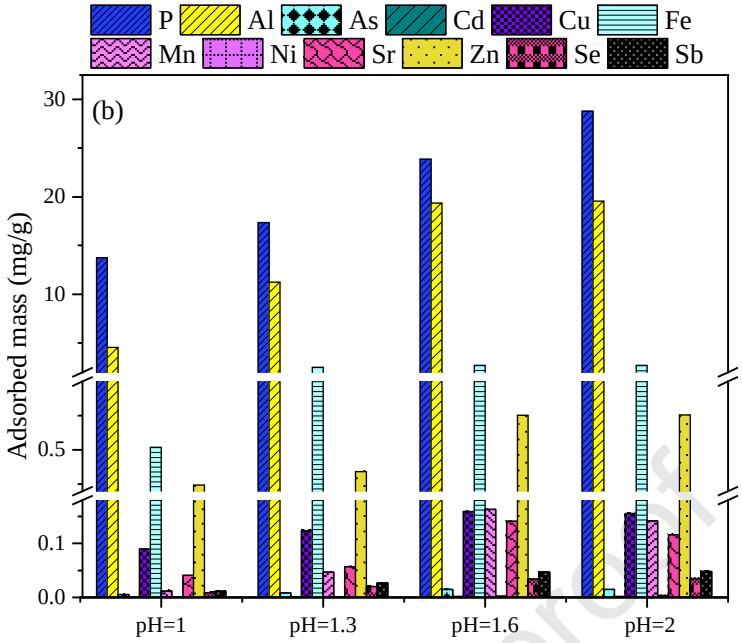

Fig. 4. Effect of initial pH of the P-extract on adsorption by ScM700 and PsM700 (a and b: P and metal(loid)s adsorption by ScM700 and PsM700, respectively)

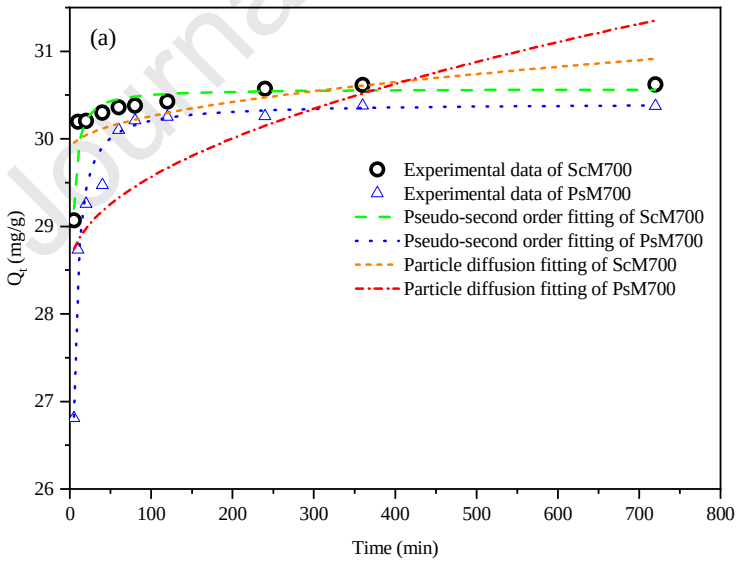

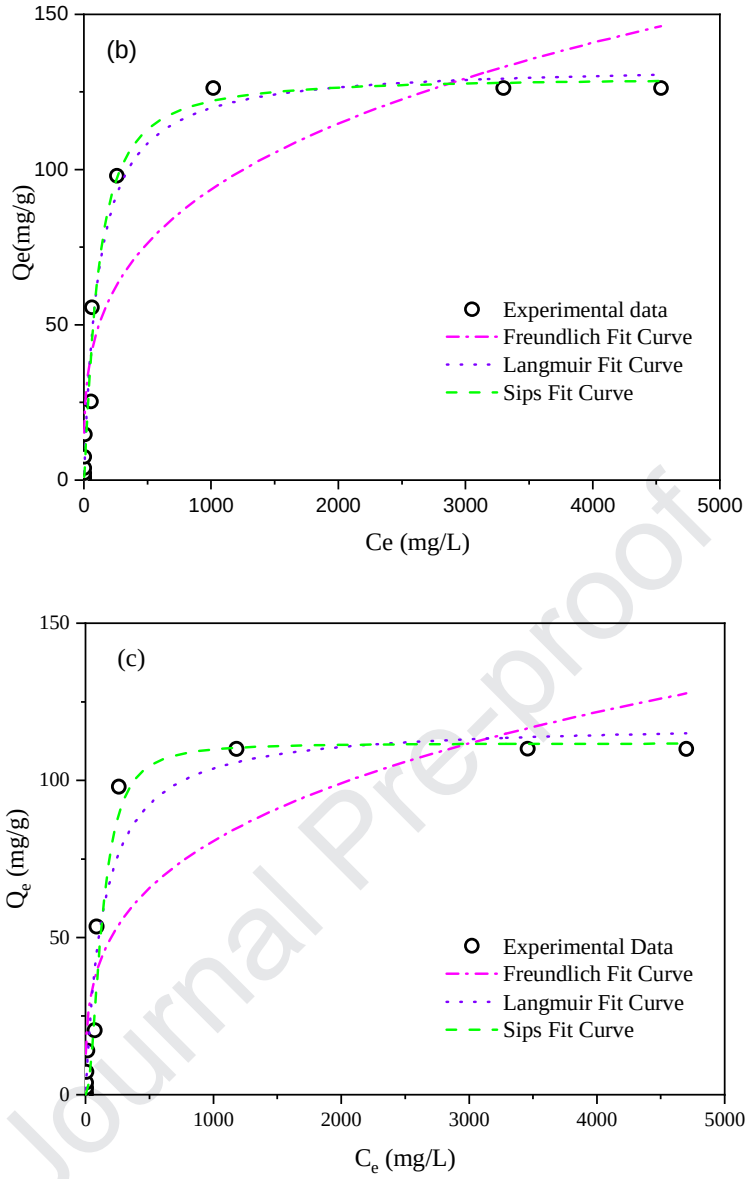

Fig. 5. Kinetic adsorption and adsorption isotherm analysis of P removal from the P-extract (a: Kinetic adsorption; b and c: adsorption isotherm analysis of ScM700 and PsM700, respectively)

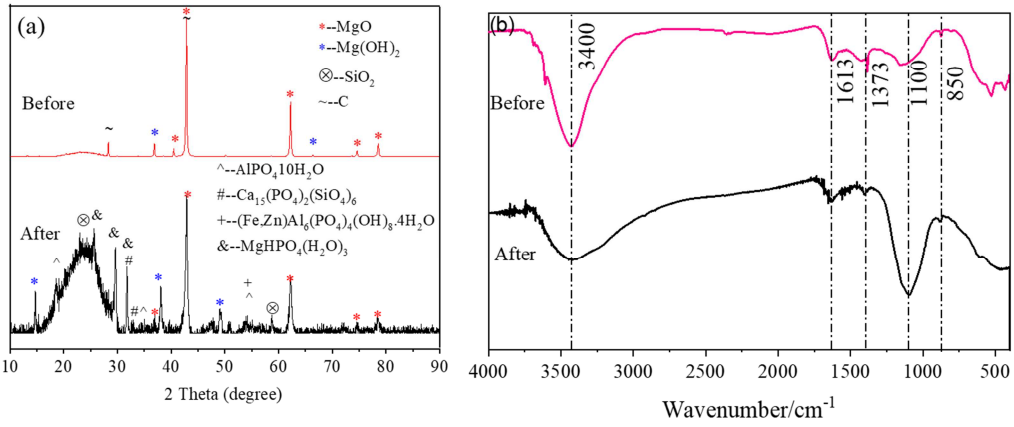

Fig. 6. XRD and FTIR spectra of ScM700 before and after absorption (a: XRD; b: FTIR)

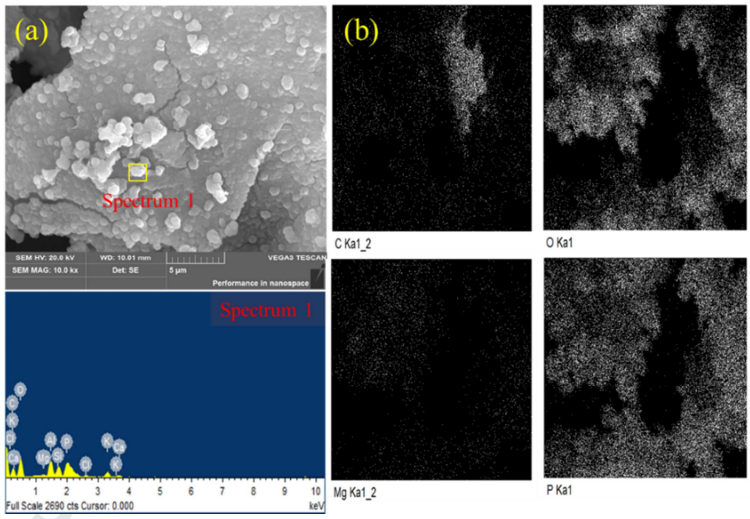

Fig. 7. SEM-EDX analysis of ScM700 after sorption (a: SEM-EDX; b: elements mapping of carbon, oxygen, magnesium, and P using EDX on SEM)

Highlights:

- P adsorption by Mg/Ca-modified biochar from acid extract of ISSA is investigated
- Biochar with high porosity and P absorption efficiency is produced
- Adsorption mechanism of P by the optimal biochar is uncovered
- The produced P-rich biochar can be used as P fertilizer